

See discussions, stats, and author profiles for this publication at: <https://www.researchgate.net/publication/260561361>

Free Energy of Lipid Bilayer Defects Affected by Alzheimer's Disease-Associated Amyloid- β 42 Monomers

ARTICLE in THE JOURNAL OF PHYSICAL CHEMISTRY B · MARCH 2014

Impact Factor: 3.3 · DOI: 10.1021/jp410477x · Source: PubMed

CITATIONS

3

READS

49

2 AUTHORS:



Tobias Pobandt

2 PUBLICATIONS 12 CITATIONS

[SEE PROFILE](#)



Volker Knecht

University of Freiburg

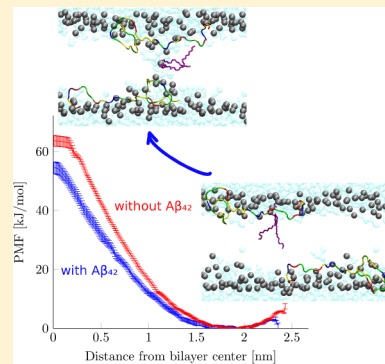
48 PUBLICATIONS 664 CITATIONS

[SEE PROFILE](#)

Free Energy of Lipid Bilayer Defects Affected by Alzheimer's Disease-Associated Amyloid- β_{42} Monomers

Tobias Pobandt[†] and Volker Knecht*,^{†,‡}[†]Theory & Bio-Systems, Max Planck Institute of Colloids and Interfaces, Science Park Golm, D-14424 Potsdam, Germany

ABSTRACT: Experimental evidence suggests that the amyloid β -peptide ($A\beta$) associated with Alzheimer's disease strongly disturbs the integrity of lipid bilayers and cell membranes, as a possible origin of the toxicity of this peptide. Here, we have used molecular dynamics simulations to compute the free energy of membrane pores in the presence and absence of $A\beta$. The validation of our approach included the calculation of lipid flip-flop waiting times, which were found to agree well with recent experiments, in contrast with an earlier simulation study that apparently overestimated these waiting times. We find that, compared with peptide-free lipid bilayers, attached $A\beta_{42}$ peptides (i) increase the order parameters of the lipid tails but (ii) decrease the effective width of the hydrophobic region, (iii) reduce the free energy and thus enlarge the density of membrane pores, and (iv) increase the lifetime of pores. A detailed understanding of the interaction of $A\beta_{42}$ with lipid bilayer membranes may assist in the design of therapeutical strategies against Alzheimer's disease.



INTRODUCTION

First described by Alois Alzheimer in 1906, the neurodegenerative Alzheimer's disease is characterized by grave memory loss and the inability to form new memories. In 2006, about 27 million elderly people were suffering from the disease worldwide. Pathological features of the disease are the deposits of senile plaques around and neurofibrillary tangles within nerve cells. The extracellular senile plaques consist of mainly amyloid- β ($A\beta$) peptides forming so-called amyloid fibrils. $A\beta$ is a 39–43 residue amphiphilic peptide derived from the integral amyloid precursor protein (APP) in an amyloidogenic pathway. $A\beta$ results from the cleavage of APP by the enzymes β - and γ -secretase.^{1,2} Most common are the 40-residue $A\beta_{40}$ and the 42-residue $A\beta_{42}$ alloforms. It is widely accepted that $A\beta$ plays a crucial role in the pathogenesis of Alzheimer's disease. Interestingly, the concentration of soluble oligomers rather than the amount of insoluble fibrils strongly correlates with the severity of the disease.^{3,4}

$A\beta$ peptides may kill nerve cells via several mechanisms, such as by generating reactive oxygen species, damaging endothelial cells, or disrupting calcium homeostasis.^{5,6} The latter might be an early step in the pathway of $A\beta$ neurotoxicity⁶ and is provoked in multiple ways, such as interaction with endogenous ion channels,^{7,8} disruption of lipid membrane integrity,⁸ or formation of selective calcium channels.⁹ It has been shown that $A\beta$ strongly interacts with cell membranes as well as lipid bilayers, leading to pore formation,^{10,11} peptide insertion,^{12,13} or membrane disruption.¹⁴ Severe local defects in membranes are small pores, which can cause increased diffusion of ions, water, or lipids through the membrane.^{15,16}

A powerful tool to illuminate interfacial binding of peptides and peptide–lipid interactions in great detail is provided by molecular dynamics (MD) simulations. MD studies have

revealed the mechanisms underlying the binding of peptides to surfaces, especially membranes, as well as the effect of lipid composition on peptide–membrane binding affinities,^{17–20} the influence of lipid–peptide interaction strengths on peptide adsorption, insertion, and the mechanism of peptide-induced pore formation.^{21–23} Especially, the lipid bilayer affinity of $A\beta$,²⁴ the effects of lipid composition on the structure²⁵ and dimerization of the peptide,²⁶ the interaction of oligomers of $A\beta$ fragments,²⁷ as well as $A\beta$ pores formed by various fragments of $A\beta$ ^{28–31} have been investigated. To our knowledge, however, to date, no MD study has focused on the effect of $A\beta$ on the free energies and, thus, the density of membrane pores.

Here, we employ MD simulations to examine the effect of $A\beta_{42}$ on pore formation in lipid bilayers. Using the umbrella sampling technique, the free energy of water pores in a DPPC bilayer at a peptide-to-lipid ratio of 2:128 is determined. The results are compared with a peptide-free reference system. Pore closure is simulated to determine pore closure and opening rates (the latter via the free energy of pore formation and detailed balance), and the dependence of the density of lipid bilayer defects on the density of bilayer attached peptides is evaluated.

From our simulations, a decrease in the free energy of membrane pores of about 9 kJ/mol due to attached $A\beta_{42}$ monomers, resulting in an increased pore density, is observed. Furthermore, we find that $A\beta_{42}$ stabilizes preformed pores kinetically. Lipid flip-flop waiting times from our simulations are in accordance with recent experiments. For the peptide-free reference system, the free energy of membrane pores is

Received: October 23, 2013

Revised: February 24, 2014

Published: March 5, 2014

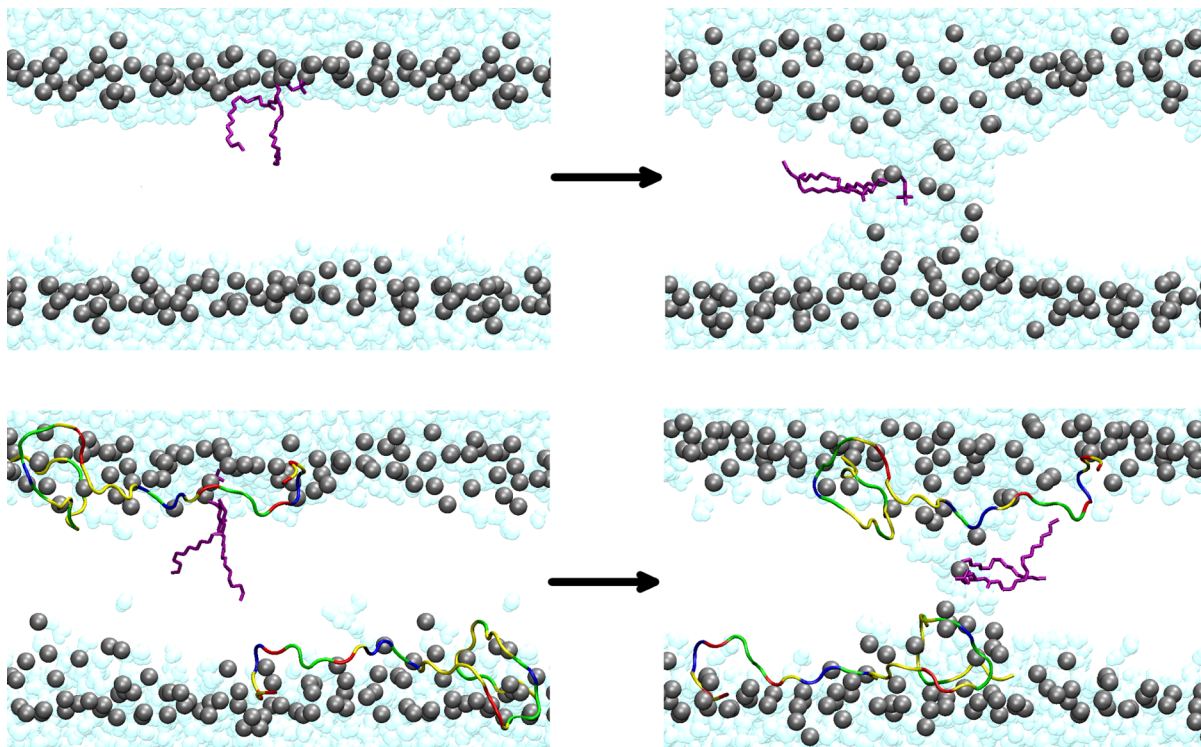


Figure 1. Pore formation for $z_L \rightarrow 0$ in the absence (top) and presence (bottom) of $A\beta_{42}$. The water molecules are shown as cyan spheres, and the lipid restrained by the umbrella potential is depicted as purple sticks. The phosphor atoms of the other lipids are shown in silver. The peptides are depicted in ribbon presentation; here, colors distinguish among basic (blue), acidic (red), hydrophobic (yellow), and hydrophilic (green) residues. For clarity, water molecules are translated to the background.

lower than estimated from a similar simulation study carried out by Tieleman and Marrink.³² The latter overestimates flip-flop waiting times compared to experiment, apparently as a result of the shorter simulation time scale employed.

METHODS

Setup. MD simulations were conducted to evaluate the free energy and lifetime of water pores in a 1,2-dipalmitoyl-sn-glycero-3-phosphocholine (DPPC) lipid bilayer. The system contained a bilayer comprising 128 lipids with an $A\beta_{42}$ monomer attached to each leaflet, denoted as *symmetric setup*. For comparison, a peptide-free system was also investigated. To determine the free energy of a water pore, the potential of mean force (PMF) on the position of the headgroup of a lipid normal to the bilayer plane and relative to the center of the bilayer was calculated using MD simulations combined with the umbrella sampling technique.³³ The reaction coordinate chosen was the distance of the phosphate group of one particular DPPC lipid from the center of the bilayer, z_L . Pulling the lipid headgroup to the center of the bilayer ($z_L \rightarrow 0$) results in pore formation, as shown in Figure 1 and as observed in previous studies.³² The initial configuration of an $A\beta_{42}$ monomer attached to a DPPC bilayer was taken from replica exchange simulations performed by Davis and Berkowitz.²⁵

We also considered an *asymmetric setup*, a peptide–bilayer system with an $A\beta_{42}$ peptide bound to only one of the bilayer leaflets, which was, in fact, the original system employed in ref 25. For this system, an extraordinary high free energy barrier for pore formation ($\Delta G \approx 94$ kJ/mol) exceeding the value for a peptide-free system was obtained. This was presumably caused by a finite size effect arising from a difference in the

effective areas per lipid, $A_{\text{Lip}} = A/N_{\text{Lip}}$ between the two leaflets. Here, A denotes the total area of the simulated bilayer patch, and N_{Lip} the number of lipids per leaflet. For the peptide-free system $A_{\text{Lip}} = 0.689 (\pm 0.011) \text{ nm}^2 \equiv A_{\text{Lip},0}$; for the symmetric setup, a smaller area per lipid of $A_{\text{Lip}} = 0.660 (\pm 0.008) \text{ nm}^2 \equiv A_{\text{Lip},\text{pp}}$; and for the asymmetric setup, $A_{\text{Lip},0} = 0.669 (\pm 0.012) \text{ nm}^2 \equiv A_{\text{Lip},\text{p0}}$ was found.

The extraordinarily high free energy barrier for the asymmetric, a single peptide-containing bilayer, might be explained as follows: The total area of the membrane in the symmetric setup, A_{pp} , is found to be reduced compared with the peptide-free system, A_0 . In the asymmetric setup, the equilibrium areas of the peptide-free, A_0 , and the peptide-decorated leaflet, $A_{\text{op}} = A_{\text{pp}}$, differ as $A_0 > A_{\text{op}}$. On the other hand, because of the boundary conditions, both leaflets must adopt the same area, A . The latter may be predicted from the excess free energy of the bilayer due to the deviation of A from the equilibrium areas of the two leaflets, ΔF , according to

$$\Delta F = \Delta F_p + \Delta F_0$$

where ΔF_p and ΔF_0 denote the excess free energies of the peptide-decorated and peptide-free leaflet, correspondingly. These are given by

$$\Delta F_p = K_A \frac{(A - A_{\text{op}})^2}{4A_0}$$

and

$$\Delta F_0 = K_A \frac{(A - A_0)^2}{4A_0}$$

where K_A denotes the area compressibility modulus of the bilayer. Here, we have neglected any possible effect of the peptide on K_A and set $A_0 \sim A_{0p}$ in the denominator. Note that the factor 4 instead of 2 in the denominators stems from the fact that the formulas here refer to monolayers, not to bilayers. The resulting equilibrium area A_{eq} may be inferred from the condition

$$\left. \frac{\partial F}{\partial A} \right|_{A=A_{eq}} = 0$$

Hence,

$$K_A \frac{(A_{eq} - A_{0p})}{2A_0} + K_A \frac{(A_{eq} - A_0)}{2A_0} = 0$$

This leads to

$$A_{eq} = \frac{(A_{0p} + A_0)}{2} \quad (1)$$

which agrees with our simulation result. This means that

$$\Delta F_p(A_{eq}) = K_A \frac{(A_{0p} - A_0)^2}{16A_0} = \Delta F_0(A_{eq})$$

That is, both leaflets have the same (positive) excess free energy, although one of them is stretched, and the other condensed.

Formally, $\Delta F = \Delta F(A, L_z)$ is a function of the area A and the box dimension perpendicular to the bilayer, L_z . The control variable in our simulations, though, is neither A nor L_z , but the pressure parallel, P_L , and normal, P_N , to the membrane. To account for this in a proper thermodynamic description, we apply the Legendre transformation,

$$G = F - A \left. \frac{\partial F}{\partial A} \right|_{L_z} - L_z \left. \frac{\partial F}{\partial L_z} \right|_A = F + (P_L + P_N)V$$

$$\Delta G = \Delta F + (P_L + P_N)\Delta V$$

connecting $\Delta F = \Delta F(A, L_z)$ with $\Delta G = \Delta G(P_L, P_N)$. As for dense fluids at $P_L = P_N = 1$ atm, the relation $P\Delta V \approx 0$ holds, and we have $\Delta G = \Delta F$. In the asymmetric setup, the peptide-free leaflet is effectively compressed. This, being inverse to stretching, is expected to hinder the formation of pores. Therefore, the free energy of pores will be larger in the asymmetric than in the symmetric setup. This effect is due to the relatively small size of the bilayer and the short simulation times. In a real system, the transmembrane lipid distribution in a DPPC bilayer is expected to adapt to the distribution of peptides on a time scale of minutes.³⁴ To avoid this finite size and time scale effect, the symmetric setup was chosen.

To each system, about 5700 water molecules and to the system containing peptides Na^+ counter-cations were added. The protonation of $\text{A}\beta_{42}$ was chosen such as to mimic a physiological pH of 7. That is, the arginine and the lysine residues were modeled as cationic, the aspartate and glutamate residues as anionic, the histidine residues as neutral, the C-terminus as deprotonated and the N-terminus as protonated, leading to a net charge of $-3e$ for the peptide. All systems were energy-minimized using the steepest descent method. The peptide-free system was equilibrated for 10 ns, and the peptide–bilayer system for 20 ns. The initial configurations for the different umbrella windows were obtained by pulling

the lipid headgroup of a selected lipid to the center of the bilayer. To precisely locate its equilibrium position, the headgroup was also pulled 3–4 Å out of the bilayer in an additional simulation. Both simulations were carried out with a pulling rate of 0.02 nm/ps and an umbrella potential of 500 kJ/(mol·nm²).

From the resulting trajectories, ~70 snapshots for the peptide-containing and for the peptide-free system were taken as initial configurations for corresponding umbrella windows. For each umbrella window, the distance between the corresponding lipid headgroup and the center of the bilayer were restrained normal to the bilayer surface using a harmonic potential with a force constant of 5000 kJ/(mol·nm²). Each setup was equilibrated for 10 ns, and data were collected from an additional 100 ns simulation. The potential of mean force was calculated using the weighted histogram analysis method (WHAM),³⁵ and the statistical errors were estimated via the Bayesian bootstrap method, both implemented in the GROMACS software package.³⁶

To determine the pore closure rate, the umbrella window with the lipid headgroup restrained at the center of the bilayer ($z_L = 0$) was employed. Both for the peptide-containing and the peptide-free system, 10 different configurations with a preformed pore were taken as starting points. After releasing the corresponding pulled lipid headgroup, the simulations were extended until the pore had closed.

For all simulations, an average temperature of 323 K, being above the main transition temperature of DPPC, was maintained via a velocity rescaling thermostat,³⁷ separately coupled to lipids, water, peptides, and counter cations, with a coupling constant of 0.1 ps. Furthermore a pressure of 1 atm normal and lateral to the bilayer was maintained using a Berendsen barostat³⁸ with a time constant of 0.5 ps. van der Waals and short-range electrostatic interactions were truncated at 0.9 nm, and the long-range electrostatic interactions were computed using the particle mesh Ewald method.³⁹ All bonds of the lipids and peptides were constrained using the LINCS algorithm,⁴⁰ allowing for a simulation time step of 2 fs. The peptides were described using the GROMOS96 force field ffG43a1,⁴¹ the lipids via parameters from Berger et al.,⁴² and the water using the SPC model.⁴³ All simulations were performed using the GROMACS 4.0 software package.^{45,46}

ANALYSIS

Lipid Order Parameters. Lipid order parameters were calculated via

$$S_z^n = \frac{3}{2} \langle \cos^2 \Theta_z^n \rangle - \frac{1}{2} \quad (2)$$

Here, Θ_z^n is the angle between the bilayer normal and the vector connecting the carbon atoms C_{n-1} and C_{n+1} , and the brackets indicate an average over molecules and time.

Pore Closure Time. The probability $P_{cl}(t)$ that a pore opened at time zero is closed at time t was estimated from

$$P_{cl}(t) \equiv P(t \geq \tau_{cl}) = \frac{q_{cl}(t)}{n} \quad (3)$$

Here, τ_{cl} denotes the pore closure time, $q_{cl}(t)$ the number of simulations exhibiting a closed pore at time t , and n the total number of simulations. $P_{cl}(t)$ is related to the probability that a given pore is still open at time t , $P_{op}(t)$, according to

$$P_{\text{cl}}(t) = 1 - P_{\text{op}}(t)$$

Assuming a Markovian process for $P_{\text{op}}(t) \equiv P(t < \tau_{\text{cl}})$ leads to

$$P_{\text{op}}(t) = \exp\left(-\frac{t}{\tau_{\text{cl}}}\right)$$

and therefore,

$$P_{\text{cl}}(t) = 1 - \exp\left(-\frac{t}{\tau_{\text{cl}}}\right) \quad (4)$$

Pore Densities for Peptide-Free Lipid Bilayer. To derive formulas to estimate pore densities, first, a peptide-free lipid bilayer will be considered. The distance of the phosphate group of a given lipid from the center of the bilayer in the z direction will be denoted as z_L . If z is fixed below a critical value, z_p , using an umbrella potential in a MD simulation, a pore forms spontaneously. It is intuitive to denote a lipid with $z_L < z_p$ as to reside in the “center” of a pore. The probability that a given lipid resides in the center of a pore, P_p , is given by

$$P_p = \exp(-\beta \cdot G_p) \quad (5)$$

Here, $\beta = 1/k_B T$, where k_B denotes Boltzmann’s constant and T is absolute temperature. The free energy of the pore, G_p , is given by

$$G_p = -k_B T \cdot \ln(Z_p/Z) \quad (6)$$

where

$$Z = \int_0^{z_c} b(z_L) dz_L \quad (7)$$

is the full partition function for a bilayer-inserted lipid, and z_c is the distance from the bilayer center above which the lipid is desorbed. The symbol $b(z)$ denotes the Boltzmann factor

$$b(z_L) = \exp(-\beta \cdot G(z_L)) \quad (8)$$

where $G(z_L)$ is the PMF along z_L as obtained from the umbrella sampling simulations of the peptide-free system. The partition function for the state “lipid resides in pore center” is given by

$$Z_p = \int_0^{z_p} b(z_L) dz \quad (9)$$

Now a macroscopic bilayer patch at macroscopic time scales is considered. If N denotes the number of lipids per leaflet, $\langle N_p \rangle$ the number of pores averaged over time, N_l the number of lipids in the center of a given pore coming from one leaflet, and $\langle N_l \rangle$ the average number of lipids in the center of pores averaged over time, the equation

$$\langle N_l \rangle = \langle N_p \rangle \cdot N_l = P_p \cdot N$$

holds. In our study, N_l was obtained from a MD simulation of a bilayer with a pore by determining the corresponding number of phosphate groups in one leaflet with distances $0-z_p$ from the center of the bilayer. If A denotes the area of the (now macroscopic) patch, a the area per lipid, and

$$\rho_p = \frac{\langle N_p \rangle}{A}$$

the number of pores per area, this leads to

$$\rho_p = \frac{\exp(-\beta \cdot G_p)}{N_l \cdot a} \quad (10)$$

Pore Densities for Peptide-Decorated Lipid Bilayer.

If, in contrast, a *peptide* is present, we first assume that the probability of a lipid residing in the center of a pore is equal for all lipids in contact with the peptide. This assumption is a rather crude approximation due to the inhomogeneity of the peptide. Accordingly, we observed that pore formation was induced only in one of three cases. This effect was taken into account as described in the Results section. The probability that a given lipid in contact with the peptide resides in the center of a pore, $P_{p,c}$ is given by eq 5, with G_p in eqs 5 and 6 replaced by $G_{p,c}$ and $G(z_L)$ in eq 8 replaced by $G_{\text{pep}}(z_L)$, where $G_{\text{pep}}(z_L)$ denotes the PMF obtained from the umbrella sampling simulations in the presence of the peptide. If $\langle N_{l,c} \rangle$ denotes the number of lipids in contact with a peptide and residing in the center of a pore averaged over time, N_c the number of lipids in contact with a peptide, and $N_{l,c}$ the number of lipids in contact with a peptide and residing in the center of a given pore, the equation

$$\langle N_{l,c} \rangle = \langle N_p \rangle \cdot N_{l,c} = \exp(-\beta \cdot G_{p,c}) \cdot N_c$$

holds. If N_{pep} is the number of peptides, $n_c = N_c/N_{\text{pep}}$ the number of lipids in contact with a single peptide, and $n_{\text{pep}} = N_{\text{pep}}/N$ the molar ratio of peptides and lipids, the pore density is

$$\rho_p = \exp(-\beta \cdot G_{p,c}) \cdot n_c \cdot \frac{n_{\text{pep}}}{a \cdot N_{l,c}}$$

In the presence of a peptide, two types of pores will be present: c-type pores denoting pores involving lipids in contact with a peptide, and n-type pores not involving lipids in contact with a peptide. If the average number of c-type pores is $\langle N_{p,c} \rangle$, the average number of n-type pores is $\langle N_{p,n} \rangle$, and the total number of pores is $\langle N_p \rangle$, then

$$\langle N_p \rangle = \langle N_{p,c} \rangle + \langle N_{p,n} \rangle$$

The number of lipids in the center of a peptide in a c-type pore will be called $N_{l,c}$ and the number of lipids in the center of an n-type pore, $N_{l,n}$. Then the number of c-type pores is given by

$$\langle N_{p,c} \rangle = \frac{N_c}{N_{l,c}} \cdot \exp(-\beta \cdot G_{p,c})$$

and the number of n-type pores by

$$\langle N_{p,n} \rangle = \frac{N - N_c}{N_{l,n}} \cdot \exp(-\beta \cdot G_{p,n})$$

Here,

$$G_{p,i} = -k_B T \cdot \ln\left(\frac{Z_{p,i}}{Z_i}\right) \quad i = c, n$$

with the partition function for the pore state,

$$Z_{p,i} = \int_0^{z_p} b_i(z) dz \quad i = c, n$$

and the full partition function for the membrane-inserted lipid,

$$Z_i = \int_0^{z_c} b_i(z) dz \quad i = c, n$$

Here, again, z_c denotes the position from which the lipid is desorbed from the bilayer, and $b_i(z)$ is the Boltzmann factor,

$$b_i(z) = \exp(-\beta \cdot G_i(z)) \quad i = c, n$$

$G_n(z)$ denoting the PMF for the peptide-free and $G_c(z)$ the PMF for the bilayer with the peptide. With

$$P_i \equiv \exp(-\beta \cdot G_{p,i}) \quad i = c, n$$

the number of pores per area is

$$\rho_p = \frac{\langle N_p \rangle}{A} = \frac{\langle N_p \rangle}{Na} = \frac{P_c \cdot n_c n_{pep}}{N_{l,c} a} + \frac{P_n (1 - n_c n_{pep})}{N_{l,n} a} \quad (11)$$

RESULTS

Pulling a selected lipid headgroup to the center of a DPPC bilayer induced the formation of a pore, as shown in Figure 1. The waiting time for pore formation in these biased simulations was 70 ns in the absence while only 5 ns in the presence of $A\beta_{42}$. In the latter case, the propensity of pore formation depended on the position of the pulled lipid relative to the peptide. Interestingly, no pore formed when a lipid adjacent to hydrophobic tail region Val40-Ala42 or between the largely hydrophobic segments Lys16-Phe19 and Ile31-Leu34 was manipulated, but pores did form when a lipid in the vicinity of the hydrophilic segment Ser8-His13 was displaced into the bilayer interior. The latter case was selected to compute the profile of the PMF on the lipid headgroup position normal to the bilayer. For each umbrella window for small z in which a pore formed, only the part of the trajectory after pore formation was considered in the calculation of the PMF.

Attached $A\beta_{42}$ Peptides Decrease Free Energy of Membrane Pores. The PMF profiles on the z position of the phosphate group of a lipid molecule normal to the bilayer are depicted in Figure 2. The PMF profiles show a minimum at $z \approx 1.8$ nm and a maximum at $z = 0$ which is lower in the presence of $A\beta$ than in the peptide-free system. The free energy of a pore in the DPPC bilayer obtained was $\Delta G_{wo} = 63.7 \pm 1.8$ kJ/mol in the absence and $\Delta G_{A\beta} = 54.5 \pm 2.0$ kJ/mol in the presence of $A\beta_{42}$.

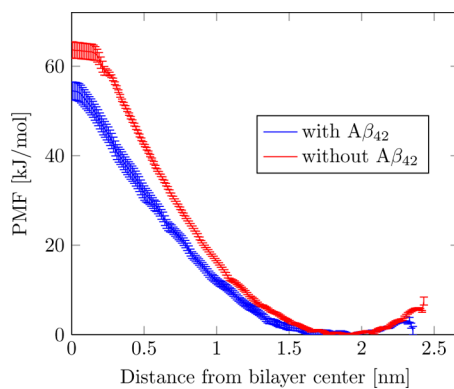


Figure 2. Potential of mean force on lipid headgroup vertically to a DPPC bilayer surface in the absence and presence of an $A\beta_{42}$ monomer attached to each leaflet of the bilayer. Pore formation takes place in the plateau for $z \rightarrow 0$.

The difference in free energy, though, is only 9 kJ/mol $\approx 3-4k_B T$, which appears relatively small. This may indicate that a strong effect on pore formation requires $A\beta$ oligomers.

$A\beta_{42}$ Increases Lifetime of Pores. When the restrained lipid headgroup in the center of a pore is released, the pore closes within 20–300 ns in the absence and within 40 ns to over 1.2 μ s in the presence of a peptide. Thus, the peptides significantly increase the lifetimes of pores. Figure 3 shows the probabilities $P_{cl}(t)$ that a pore open at time 0 is closed at time t from the simulation according to eq 3. The points are given at the times when a pore closed in one of the simulations starting from a preformed pore, and the line shows a fit of eq 4 to the data.

By means of the Wilson score method⁴⁷ an interval $[P_{cl}^-, P_{cl}^+]$ for $P_{cl}(t)$ with a confidence level of 95% was determined. Fitting eq 3 to this data yields upper and lower bounds for the average lifetime of pores, τ_{cb}

$$51 \text{ ns} \leq \tau_{cl} \leq 92 \text{ ns} \quad \text{in the absence and}$$

$$300 \text{ ns} \leq \tau_{cl} \leq 1800 \text{ ns} \quad \text{in the presence of the peptide}$$

The χ^2 value of each fit is below 0.05.

$A\beta_{42}$ Increases Pore Density. The density of pores was computed via eq 10 for the pure and via eq 11 for the peptide attached bilayer. Because our simulations do not include lipid desorption and to determine the full partition function for the bilayer inserted state of the lipid, our data were extrapolated by fitting a harmonic function to the part of the profile where no pore formation took place. The approximation of the potential of mean force by a harmonic function is appropriate, as suggested by results from Tielemans and Marrink.³² Figure 4 shows the extrapolated Boltzmann factors. Previous MD studies reported free energies for lipid desorption from pure DPPC lipid bilayers of $\Delta G_c = 75 - 80$ kJ/mol³² and $\Delta G_c = 63 \pm 4$ kJ/mol,⁴⁸ respectively. To obtain the full partition function via eq 7, the Boltzmann factor was integrated up to a phosphorus atom z coordinate corresponding to a lipid desorption free energy of $\Delta G_c = 63$ kJ/mol. The results are rather insensitive to the particular choice, though, because the Boltzmann weight already drops below 10^{-4} for a z value associated with about $\Delta G_c = 30$ kJ/mol.

For the pure bilayer, pore formation was observed when the phosphorus atom was fixed closer than $\Delta z = 0.3$ nm from the bilayer center, whereas in the presence of the peptide, pore formation required $\Delta z \leq 0.1$ nm. From the number densities of phosphorus atoms, the number of lipids involved in a single pore was evaluated to $N_L = 2.5$ for the peptide-free system and to $N_L = 0.1$ in the presence of the peptide. To determine the number of lipids in contact with the peptide, N_c , the number of lipid headgroup phosphorus atoms closer to the peptide than the pulled lipid headgroup was counted to $N_c = 35$. Because pore formation was induced only by pulling one out of three lipid head groups into the vicinity of the peptide, N_c was divided by 3. The ratio of peptides per lipid, $n_{pep} = 1/64$, and the lower and upper error bounds of the corresponding potential of mean force lead to the pore densities is

$$\rho_p = 1.8 \pm 3.6 \cdot 10^3 \text{ cm}^{-2} \quad \text{for the peptide-free system and}$$

$$\rho_p = 1.2 \pm 1.4 \cdot 10^5 \text{ cm}^{-2} \quad \text{for the system containing the peptide}$$

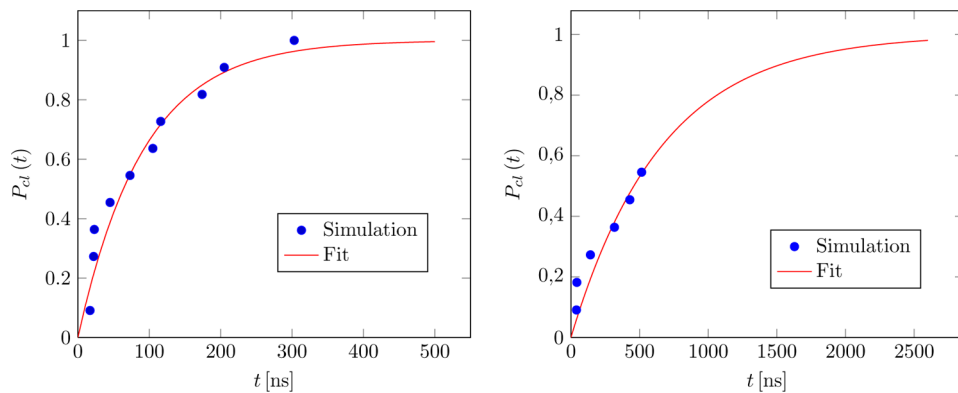


Figure 3. $P_{cl}(t)$ from simulation and fits of eq 4 for the peptide-free system (left) and in the presence of the peptide (right).

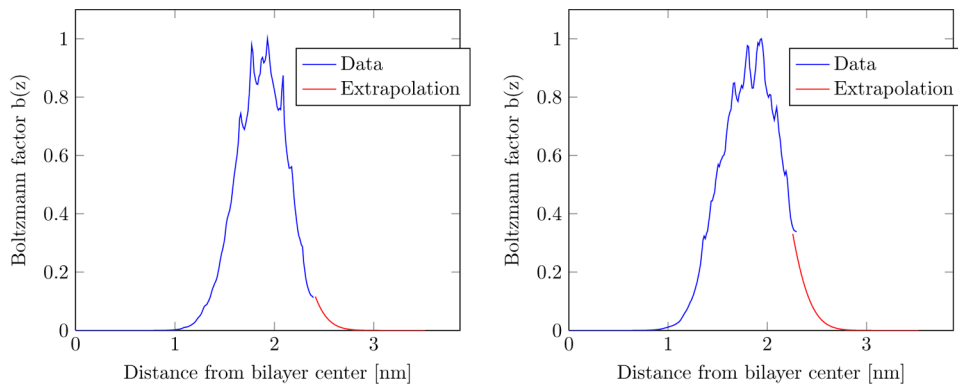


Figure 4. The Boltzmann factor as obtained from eq 8 for the peptide-free system (left) and in the presence of the peptide (right).

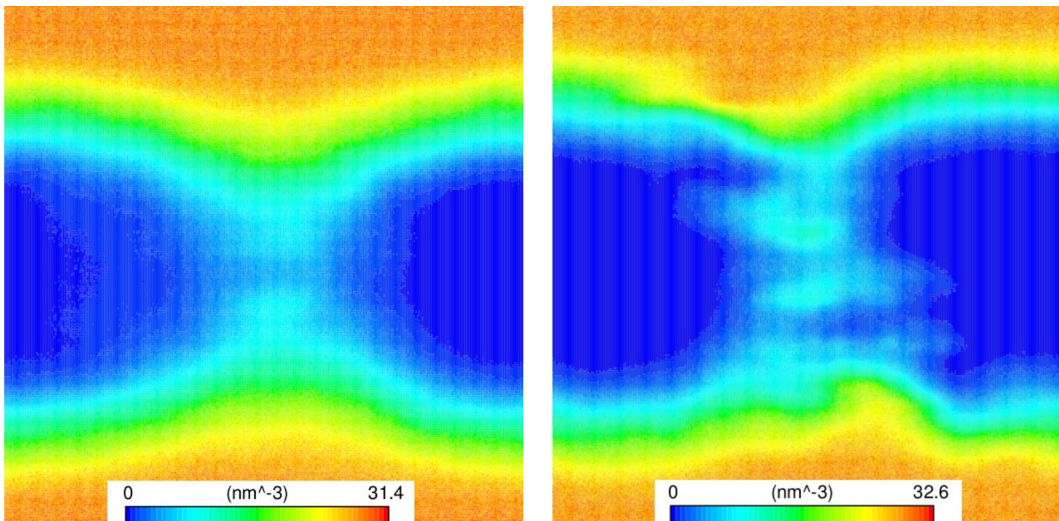


Figure 5. Number density map of water in the $x-z$ plane averaged over the 90 ns when a pore is formed. The densities are averaged over 2 nm in the y direction with the pulled lipid headgroup centered in the slice (without (left) and with $A\beta_{42}$ (right)).

$A\beta_{42}$ Monomers Lower Water and Lipid Flux through Nanopores. To compare the size of the water pores, the number of water molecules inside the pore and their flux through the pore was calculated using the software tools *g_count* and *g_flux* by Oliver Beckstein.⁴⁹ The water molecules between the centers of mass of the phosphorus atoms of the two leaflets in presence and in absence of a pore were counted, and the results in absence of the pore were subtracted from the results in presence of the pore. The number of water molecules inside a pore was thus determined

to 375 for the peptide-free system and 195 for the system containing the peptide. The flux, j , was defined as the number of water molecules entering the interior of the bilayer through one leaflet and leaving it through the other leaflet. This yielded $j = 20 \text{ ns}^{-1}$ in the absence and $j = 0.4 \text{ ns}^{-1}$ in the presence of the peptide. Although three lipid flip-flops through the bilayer spanning pore within 30 ns were detected, no lipid flip-flops within 100 ns were observed for the system containing the peptide. For the peptide-free case, this agrees

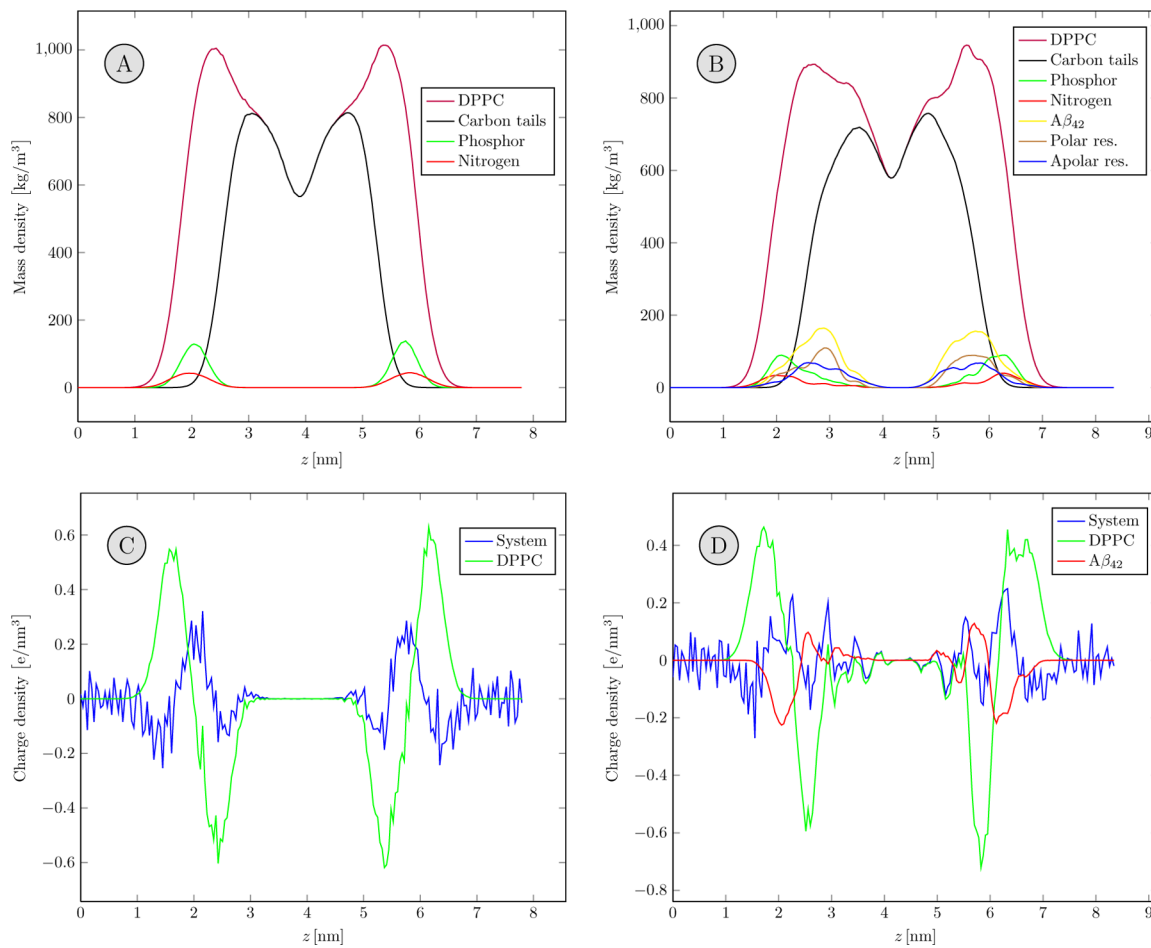


Figure 6. Mass (A, B) and charge (C, D) densities in absence (A, C) and presence (B, D) of $\text{A}\beta_{42}$ averaged over 40 ns.

well with results from molecular dynamics simulation studies of vesicle formation⁵⁰ and pore mediated lipid flip-flops.⁵¹

The difference in the size of the pores is also apparent from the configurations shown in Figure 1, whereas the shapes are illustrated as water density maps given in Figure 5. In the case of the peptide-free system, an hourglass shape of a hydrophilic pore is observed. For the peptide-containing system, the formed pore exhibits a rather disordered toroidal shape.

$\text{A}\beta_{42}$ Attachment Induces Increased Penetration of Polar Groups into the Bilayer. The mass density profile given in Figure 6B indicates that the $\text{A}\beta_{42}$ monomers deeply intrude into the hydrophobic tail region of the bilayer. Furthermore, the attachment of the peptides leads to a disturbance of the bilayer headgroup region. This is indicated from the standard deviation of the z positions of the phosphor atoms, which is 0.03 nm in the absence but 0.3 nm in the presence of the peptide. Figure 6A,B shows that the distribution of headgroup phosphor atoms broadens normal to the bilayer due to the peptides attached.

This disturbance of the headgroup region leads to a penetration of the polar headgroups into the nonpolar tail region of the bilayer. Consequently the local thickness of the nonpolar region within the bilayer decreases as a result of the attached peptide. This effect is enlarged by the intrusion of the peptide and its polar and charged residues into the hydrophobic core of the bilayer and is indicated from the charge distributions normal to the bilayer, which show a region around the bilayer center where the charge density is

identical to zero, as depicted in Figure 6C,D. The width of this region is ~ 2 nm for the peptide-free system but only ~ 0.5 nm in the presence of the peptide.

Thus, even in the absence of the pore, the peptide causes an increased penetration of polar groups into the bilayer. Hence, the pore-free and the pore state are less different from that in the absence of the peptide. This is presumably the reason why in the presence of the peptide, a pore is more probable.

To elucidate the effect of the peptide on the overall bilayer thickness, the latter was defined as the difference in the average z position of the phosphor atoms of the two leaflets, d , and the error was taken as the standard deviation of d over the simulation time. This yielded $d = 3.64 (\pm 0.05)$ nm in the absence and $d = 3.75 \pm 0.04$ nm in the presence of the peptide. Thus, the peptide is observed to lead to an increase in the global bilayer thickness.

$\text{A}\beta_{42}$ Increases Order Parameters of Lipid Hydrocarbon Tails. An increase in the bilayer thickness upon addition of peptides is expected to correlate with a corresponding increase in the order parameters of the lipid tails, S_z^n . The effect of pores and peptides on S_z^n from eq 2 is shown in Figure 7. All order parameters are positive, which means that all tail segments are preferentially oriented normal to the bilayer plane. The order parameters are highest close to the lipid headgroups (small n) and decrease toward the tips of the tails.

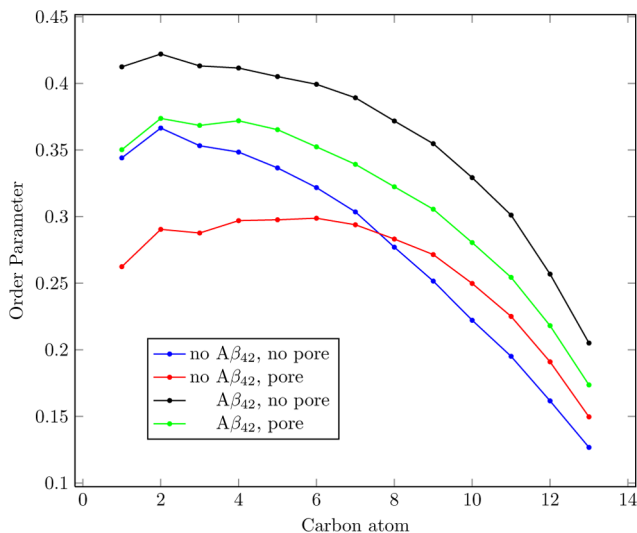


Figure 7. Order parameters averaged over 10 ns in the presence and absence of peptide and pore.

For the peptide-free bilayer, pore formation leads to a decrease in S_z^n close to the headgroups ($1 \leq n \leq 7$). This is expected because the tails of lipids surrounding the center of the water pore are more parallel to the bilayer plane than for the other lipids. Toward the tips of the tails ($8 \leq n \leq 13$), though, pore formation leads to an increase in S_z^n .

As expected from the increase in bilayer thickness observed in the presence of $A\beta$ compared with the peptide-free case, addition of $A\beta$ leads to an overall increase in S_z^n in both the absence and presence of a pore. In the presence of the peptide, pore formation leads to an increase in S_z^n for all n .

DISCUSSION

An explanation for the decrease in the free energy of membrane pores due to attached $A\beta_{42}$ monomers is given by the effect of the peptide on the nonpolar bilayer center region, as pointed out in the Results section. The free energy needed to force a polar lipid headgroup into the nonpolar tail region is expected to decrease with the effective width of this region, which, indeed, is found to be smaller in the presence than in the absence of the peptide.

The free energy of a pore in the peptide-free bilayer, ΔG , estimated here is markedly different from the value obtained via similar simulations by Tieleman and Marrink:³² our work yields $\Delta G = 64$ kJ/mol; Tieleman and Marrink obtained $\Delta G = 75\text{--}80$ kJ/mol. The main reason for this discrepancy appears to be the underestimation of the pore state in ref 32 due to shorter production runs employed, as explained in the following. The PMF increases if a lipid headgroup approaches the center of the bilayer until a critical distance is reached at which point the pore state appears to be more stable than the pore-free state, as indicated from the fact that fixing a lipid headgroup at this distance leads to the spontaneous formation of a pore. In the distance range where the pore state is the most stable state, the PMF shows a plateau. This means that the estimate of ΔG in fact depends on the width of the plateau region, which in our study is 0.2 nm. In our simulations, pore formation in the umbrella windows corresponding to the right edge of the plateau in the PMF was observed after more than 50 ns, corresponding to the

simulation time chosen in ref 32, whereas the time scale chosen in our study was about 100 ns.

Thus, it could well be that for some distances of the restrained lipid headgroup from the bilayer center for which pore formation was observed in our work, no pores formed in ref 32, leading to higher values for ΔG . Indeed, in ref 32, essentially no plateau region for small values of z_L was observed, and pores formed only for $z_L = 0$. Furthermore, because the pore state seems to be much more stable and thus, highly preferred, it can be assumed that on long time scales, the pore-free state can be neglected in the determination of the free energy of membrane pores. Hence, in our simulations, only the part of the trajectories corresponding to the pore state was considered for the calculation of the PMF.

Supporting the importance of pore formation on the PMF, taking into account only the parts of the trajectories where no pore is present yielded a free energy of $\text{PMF}(z = 0) = 78$ kJ/mol, similar to the value found in ref 32, whereas $\text{PMF}(z = 0) = 64$ kJ/mol was obtained if only the parts of the trajectories exhibiting a hydrophilic pore were employed in the analysis. To check the convergence of our simulations, we extended the trajectory of the umbrella window as close as possible to the bilayer center without formation of a water pore to 500 ns. Thereby, we ensured that the whole range of the reaction coordinate where pore formation takes place was included. Although, in addition, in ref 32 a smaller bilayer patch of 64 DPPC lipids was considered, the previous analyses showed that the difference in the results can be explained sufficiently by a difference in the simulation time scales and that, therefore, finite size effects might not play a crucial role in the observed discrepancy.

We note, though, that the estimate for the free energy of the pore state obtained from our simulations, $\Delta G_{p,\text{MD}}$, is, in fact, an upper bound for the real value, $\Delta G_{p,\infty}$. This is because the initial state employed in the simulations is pore-free. Whether for a given position z_L of the lipid headgroup a pore forms during the simulations will depend on the time scale employed, which, on the other hand, is restricted because of the huge computational expense of the calculations. We cannot exclude that at some positions z_L close to the membrane center where no pore is formed on the time scales currently used, a pore may form on longer time scales. The latter event would lead to a decrease in $\Delta G_{p,\text{MD}}$. Hence, the value $\Delta G_{p,\text{MD}} \geq \Delta G_{p,\infty}$.

However, to compare our results with experiments, the lipid flip-flop waiting time was computed from

$$\tau = \frac{1}{J} \quad (12)$$

where $J = j\rho_{\text{pore}}$ denotes the flux of particles through the bilayer, j the flux through a single pore, and ρ_{pore} the pore density. For the peptide-free system, three lipid flips were observed during 30 ns, and thus, $j = 0.1 \text{ ns}^{-1}$, leading to a flip waiting time of $\tau = (2.71 - 8.12) \times 10^2 \text{ s}$. Accordingly, flip-flop times are in the range $5 \text{ min} \leq \tau_{\text{Lip}} \leq 14 \text{ min}$. Vibrational sum-frequency generation (VSFG) spectroscopy experiments considering planar supported bilayers of DPPC lipids³⁴ yielded a half-life of lipid flip-flops of 9.2 min,³⁴ thus, within the range of our estimate.

It should be noted, though, that our simulations were carried out at 323 K, thus, above the phase transition of free-standing DPPC bilayers at 314 K.⁵² The VSFG spectroscopy

experiments were conducted at 310 K, thus, below but close to the phase transition of free-standing DPPC bilayers. However, supported bilayers are typically under tension, which is expected to lower the main transition temperature such that the DPPC bilayers probed in ref 34 were most likely in the fluid phase. Hence, the good agreement of the flip-flop times between these experiments and our simulation may not be coincidental. Our results support the view that pore formation is the rate-limiting step of lipid flip-flops.⁵¹ On the other hand, Tieleman and Marrink's MD simulations yielded $\tau_{\text{Lip}} = 30$ h, thus strongly overestimating the flip-flop time, apparently because of the overestimation of ΔG and the resulting underestimation of ρ_{pore} .

The water permeability was estimated from

$$P = \frac{J}{\Delta C}$$

where ΔC denotes the concentration difference. Assuming $\Delta C = 55$ M and using the flux $j = 20$ ns⁻¹ in the absence and $j = 0.4$ ns⁻¹ in the presence of the peptide, pore-mediated water permeabilities of $P \approx 1.1 \times 10^{-9}$ cm/s in the absence and a comparable value of $P \approx 1.4 \times 10^{-9}$ cm/s at a peptide–lipid ratio of 1:64 are obtained. Overall, water permeability coefficients for pure DPPC bilayers were reported to cover a range of $P = 10^2$ – 10^4 cm/s from simulations^{53,54} as well as from experiments.^{55,56} Water permeation is therefore confirmed not to be pore-mediated.

On the basis of the pore closure rates, $k_{\text{cl}} = \tau_{\text{cl}}^{-1}$, the pore formation rate, k_f , is calculated via detailed balance as

$$k_f = k_{\text{cl}} \cdot \exp\left(\frac{-\Delta G}{k_B T}\right)$$

This yields 4.0×10^{10} s⁻¹ cm⁻² $\leq k_f \leq 2.8 \times 10^{11}$ s⁻¹ cm⁻² in the absence of peptides and 6.2×10^{10} s⁻¹ cm⁻² $\leq k_f \leq 1.7 \times 10^{12}$ s⁻¹ cm⁻² at a peptide–lipid ratio of 1:64. Attached A β peptides thus tend to increase the pore formation rate. Pore formation rates in the presence and absence of A β could be estimated experimentally by dynamic tension spectroscopy experiments.⁵⁷

CONCLUSION

In summary, our results show that A β_{42} monomers strongly interact with zwitterionic lipid bilayers, leading to thermodynamic and kinetic stabilization of bilayer defects such as water pores. We presented results for free energies as well as closure times of small water pores. Our study opens the perspective to investigate the effect of more toxic species, such as dimers or small oligomers of A β_{42} on pore formation and closure.

AUTHOR INFORMATION

Corresponding Author

*E-mail: volker.knecht@physik.uni-freiburg.de.

Present Address

[‡](V.K.) Biomolecular Dynamics, Institute of Physics, Albert Ludwigs University, Hermann-Herder Straße 3, D-79104 Freiburg, Germany. Phone: +49-761-203-5913.

Notes

The authors declare no competing financial interest.

ACKNOWLEDGMENTS

Financial support from the Deutsche Forschungsgemeinschaft (DFG) via the IGRTG 1524 is gratefully acknowledged. We thank Max L. Berkowitz and Sheeba J. Irudayam for fruitful discussions and comments, as well as Charles Davis for providing the initial configurations of the peptides.

REFERENCES

- Kang, J.; Lemaire, H. G.; Unterbeck, A.; Salbaum, J. M.; Masters, C. L.; Grzeschik, K. H.; Multhaup, G.; Beyreuther, K.; Mullerhill, B. The Precursor of Alzheimer's-Disease Amyloid-A4 Protein Resembles a Cell-Surface Receptor. *Nature* **1987**, *325*, 733–736.
- Miller, D. L.; Papayannopoulos, I. A.; Styles, J.; Bobin, S. A.; Lin, Y. Y.; Biemann, K.; Iqbal, K. Peptide Compositions of the Cerebrovascular and Senile Plaque Core Amyloid Deposits of Alzheimer's-Disease. *Arch. Biochem. Biophys.* **1993**, *301*, 41–52.
- Lue, L. F.; Kuo, Y. M.; Roher, A. E.; Brachova, L.; Shen, Y.; Sue, L.; Beach, T.; Kurth, J. H.; Rydel, R. E.; Rogers, J. Soluble Amyloid β Peptide Concentration as a Predictor of Synaptic Change in Alzheimer's Disease. *Am. J. Pathol.* **1999**, *155*, 853–862.
- Näslund, J.; Haroutunian, V.; Mohs, R.; Davis, K. L.; Davies, P.; Greengard, P.; Buxbaum, J. D. Correlation Between Elevated Levels of Amyloid Beta-Peptide in the Brain and Cognitive Decline. *J. Am. Med. Assoc.* **2000**, *283*, 1571–1577.
- Rauk, A. Why is the Amyloid Beta Peptide of Alzheimer's Disease Neurotoxic? *Dalton Trans.* **2008**, *10*, 1273–1282.
- Kawahara, M.; Ohtsuka, I.; Yokoyama, S.; Kato-Negishi, M.; Sadakane, Y. Membrane Incorporation, Channel Formation, and Disruption of Calcium Homeostasis by Alzheimer's β -Amyloid Protein. *Int. J. Alzh. Dis.* **2011**, *2011*, 1–17.
- Rovira, C.; Arbez, N.; Mariani, J. A β (25–35) and A β (1–40) Act on Different Calcium Channels in CA1 Hippocampal Neurons. *Biochem. Biophys. Res. Commun.* **2002**, *296*, 1317–1321.
- Demuro, A.; Parker, I.; Stutzmann, G. E. Calcium Signaling and Amyloid Toxicity in Alzheimer Disease. *J. Biol. Chem.* **2010**, *285*, 12463–12468.
- Arispe, N.; Diaz, J. C.; Simakova, O. A β Ion Channels. Prospects for Treating Alzheimer's Disease with A β Channel Blockers. *Biochim. Biophys. Acta* **2007**, *1768*, 1952–1965.
- Arispe, N.; Pollard, H. B.; Rojas, E. Giant Multilevel Cation Channels Formed by Alzheimer Disease Amyloid β -Protein [A β P-(1–40)] in Bilayer Membranes. *Proc. Natl. Acad. Sci. U.S.A.* **1993**, *90*, 10573–10577.
- Alarcon, J. M.; Brito, J. A.; Hermosilla, T.; Atwater, I.; Mears, D.; Rojas, E. Ion Channel Formation by Alzheimer's Disease Amyloid Beta-Peptide (Abeta40) in Unilamellar Liposomes is Determined by Anionic Phospholipids. *Peptides* **2006**, *27*, 95–104.
- Terzi, E.; Hölzemann, G.; Seelig, J. Interaction of Alzheimer β -Amyloid Peptide (1–40) with Lipid Membranes. *Biochem.* **1997**, *36*, 14845–14852.
- Curtai, C. C.; Ali, F. E.; Smith, D. G.; Bush, A. I.; Masters, C. L.; Barnham, K. J. Metal Ions, pH, and Cholesterol Regulate the Interactions of Alzheimer's Disease Amyloid–Beta-Peptide with Membrane Lipid. *J. Biol. Chem.* **2003**, *278*, 2977–2982.
- Ambroggio, E. E.; Kim, D. H.; Separovic, F.; Barrow, C. J.; Barnham, K. J.; Bagatolli, L. A.; Fidelio, G. D. Surface Behavior and Lipid Interaction of Alzheimer Beta-Amyloid Peptide 1–42: A Membrane-Disrupting Peptide. *Biophys. J.* **2005**, *88*, 2706–2713.
- Leontiadou, H.; Mark, A. E.; Marrink, S. J. Ion Transport across Transmembrane Pores. *Biophys. J.* **2007**, *92*, 4209–4215.
- Hamilton, R.; Kaler, E. Alkali Metal Ion Transport through Thin Bilayers. *J. Phys. Chem.* **1990**, *94*, 2560–2566.
- Horinek, D.; Serr, A.; Geisler, M.; Pirzer, T.; Slotta, U.; Lud, S. Q.; Garrido, J. A.; Scheibel, T.; Hugel, T.; Netz, R. R. Peptide Adsorption on a Hydrophobic Surface Results from an Interplay of Solvation, Surface, and Intrapptide Forces. *Proc. Natl. Acad. Sci.* **2008**, *105*, 2842–2847.

- (18) von Deuster, C. I. E.; Knecht, V. Antimicrobial Selectivity Based on Zwitterionic Lipids and Underlying Balance of Interactions. *Biochim. Biophys. Acta* **2012**, *1818*, 2192–2201.
- (19) von Deuster, C. I. E.; Knecht, V. Competing Interactions for Antimicrobial Selectivity Based on Charge Complementarity. *Biochim. Biophys. Acta* **2011**, *1808*, 2867–2876.
- (20) Vivcharuk, V.; Tomberli, B.; Tolokh, I. S.; Gray, C. G. Prediction of Binding Free Energy for Adsorption of Antimicrobial Peptide Lactoferricin B on a POPC Membrane. *Phys. Rev. E* **2008**, *77*, 031913.
- (21) Leontiadou, H.; Mark, A. E.; Marrink, S. J. Antimicrobial Peptides in Action. *J. Am. Chem. Soc.* **2006**, *128*, 12156–12161.
- (22) Sengupta, D.; Leontiadou, H.; Mark, A. E.; Marrink, S. J. Toroidal Pores Formed by Antimicrobial Peptides Show Significant Disorder. *Biochim. Biophys. Acta, Biomembr.* **2008**, *1778*, 2308–2317.
- (23) Rzepiela, A. J.; Sengupta, D.; Goga, N.; Marrink, S. J. Membrane Poration by Antimicrobial Peptides Combining Atomistic and Coarse-Grained Descriptions. *Faraday Discuss.* **2010**, *144*, 431–443.
- (24) Davis, C. H.; Berkowitz, M. L. Interaction between Amyloid-Beta (1–42) Peptide and Phospholipid Bilayers: A Molecular Dynamics Study. *Biophys. J.* **2009**, *96*, 785–797.
- (25) Davis, C. H.; Berkowitz, M. L. Structure of the Amyloid-Beta (1–42) Monomer Absorbed to Model Phospholipid Bilayers: A Molecular Dynamics Study. *J. Phys. Chem. B* **2009**, *113*, 14480–14486.
- (26) Davis, C. H.; Berkowitz, M. L. A Molecular Dynamics Study of the Early Stages of Amyloid-Beta(1–42) Oligomerization: The Role of Lipid Membranes. *Proteins: Struct., Funct. Bioinf.* **2010**, *78*, 2533–2545.
- (27) Yu, X.; Wang, Q.; Pan, Q.; Zhou, F.; Zheng, J. Molecular Interactions of Alzheimer Amyloid- β Oligomers with Neutral and Negatively Charged Lipid Bilayers. *Phys. Chem. Chem. Phys.* **2013**, *15*, 8878–8889.
- (28) Jang, H.; Zheng, J.; Nussinov, R. Models of Beta-Amyloid Ion Channels in the Membrane Suggest that Channel Formation in the Bilayer is a Dynamic Process. *Biophys. J.* **2007**, *93*, 1938–1949.
- (29) Jang, H.; Zheng, J.; Lal, R.; Nussinov, R. New Structures Help the Modeling of Toxic Amyloid β Ion Channels. *Trends Biochem. Sci.* **2008**, *33*, 91–100.
- (30) Jang, H.; Arce, F. T.; Ramachandran, S.; Capone, R.; Lal, R.; Nussinov, R. Structural Convergence among Diverse, Toxic β -Sheet Ion Channels. *J. Phys. Chem. B* **2010**, *114*, 9445–9451.
- (31) Jang, H.; Arce, F. T.; Ramachandran, S.; Capone, R.; Azimova, R.; Kagan, B. L.; Nussinov, R.; Lal, R. Truncated β -Amyloid Peptide Channels Provide an Alternative Mechanism for Alzheimer's Disease and Down Syndrome. *Proc. Natl. Acad. Sci.* **2010**, *107*, 6538–6543.
- (32) Tieleman, D. P.; Marrink, S. J. Lipids out of Equilibrium: Energetics of Desorption and Pore Mediated Flip-Flop. *J. Am. Chem. Soc.* **2006**, *128*, 12462–12467.
- (33) Torrie, G. M.; Valleau, J. P. Nonphysical Sampling Distributions in Monte Carlo Free-Energy Estimation: Umbrella Sampling. *J. Comput. Phys.* **1977**, *23*, 187–199.
- (34) Liu, J.; Conboy, J. C. 1,2-Diacyl-phosphatidylcholine Flip-Flop Measured Directly by Sum-Frequency Vibrational Spectroscopy. *Biophys. J.* **2005**, *89*, 2522–2532.
- (35) Kumar, S.; Rosenberg, J. M.; Bouzida, D.; Swendsen, R. H.; Kollman, P. A. The Weighted Histogram Analysis Method for Free-Energy Calculations on Biomolecules. I. The Method. *J. Comput. Chem.* **1992**, *13*, 1011–1021.
- (36) Hub, J. S.; de Groot, B. L.; van der Spoel, D. g_wham—A Free Weighted Histogram Analysis Implementation Including Robust Error and Autocorrelation Estimates. *J. Chem. Theor. Comput.* **2010**, *6*, 3713–3720.
- (37) Bussi, G.; Donadio, D.; Parrinello, M. Canonical Sampling through Velocity Rescaling. *J. Chem. Phys.* **2007**, *126*, 014101.
- (38) Berendsen, H. J. C.; Postma, J. P. M.; van Gunsteren, W. F.; DiNola, A.; Haak, J. R. Molecular Dynamics with Coupling to an External Bath. *J. Chem. Phys.* **1984**, *81*, 3684–3690.
- (39) Essmann, U.; Perera, L.; Berkowitz, M. L.; Darden, T.; Lee, H.; Pedersen, L. A Smooth Particle Mesh Ewald Method. *J. Chem. Phys.* **1995**, *103*, 8577–8593.
- (40) Hess, B.; Bekker, H.; Berendsen, H. J. C.; Fraaije, J. G. E. M. LINCS: A Linear Constraint Solver for Molecular Simulations. *J. Comput. Chem.* **1997**, *18*, 1463–1472.
- (41) van Gunsteren, W. F.; Billeter, S. R.; Eising, A. A.; Hünenberger, P. H.; Krüger, P.; Mark, A. E.; Scott, W. R. P.; Tironi, I. G. *Biomolecular Simulation: The GROMOS96 Manual and User Guide*; Hochschulverlag an der ETH Zürich: Zürich, CH, 1996.
- (42) Berger, O.; Edholm, O.; Jähnig, F. Molecular Dynamics Simulations of a Fluid Bilayer of Dipalmitoylphosphatidylcholine at Full Hydration, Constant Pressure, and Constant Temperature. *Biophys. J.* **1997**, *72*, 2002–2013.
- (43) Berendsen, H. J. C.; Postma, J. P. M.; van Gunsteren, W. F.; Hermans, J. *Intermolecular Forces*; Pullman, B., Ed.; Reidel: Dordrecht, NL, 1981; pp 331–342.
- (44) van der Spoel, D.; Lindahl, E.; Hess, B.; Groenhof, G.; Mark, A. E.; Berendsen, H. J. C. GROMACS: Fast, Flexible, and Free. *J. Comput. Chem.* **2005**, *26*, 1701–1718.
- (45) Hess, B.; Kutzner, C.; van der Spoel, D.; Lindahl, E. GROMACS 4: Algorithms for Highly Efficient, Load-Balanced, and Scalable Molecular Simulation. *J. Chem. Theor. Comput.* **2008**, *4*, 435–447.
- (46) Berendsen, H. J. C.; van der Spoel, D.; van Drunen, R. GROMACS - A Message-Passing Parallel Molecular-Dynamics Implementation. *Comp. Phys. Commun.* **1995**, *91*, 43–56.
- (47) Wilson, E. B. Probable Inference, the Law of Succession, and Statistical Inference. *J. Am. Stat. Assoc.* **1927**, *22*, 209–212.
- (48) Grafmüller, A.; Lipowsky, R.; Knecht, V. Effect of Tension and Curvature on the Chemical Potential of Lipids in Lipid Aggregates. *Phys. Chem. Chem. Phys.* **2012**, *15*, 876–881.
- (49) Beckstein, O.; Sansom, M. S. P. The Influence of Geometry, Surface Character, and Flexibility on the Permeation of Ions and Water through Biological Pores. *Phys. Biol.* **2004**, *1*, 42–52.
- (50) de Vries, A. H.; Mark, A. E.; Marrink, S. J. Molecular Dynamics Simulation of the Spontaneous Formation of a Small DPPC Vesicle in Water in Atomistic Detail. *J. Am. Chem. Soc.* **2004**, *126*, 4488–4489.
- (51) Gurtovenko, A. A.; Vattulainen, I. Molecular Mechanism for Lipid Flip-Flops. *J. Phys. Chem. B* **2007**, *111*, 13554–13559.
- (52) Koynova, R.; Caffrey, M. Phases and Phase Transitions of the Phosphatidylcholines. *Biochim. Biophys. Acta* **1998**, *1376*, 91–145.
- (53) Marrink, S. J.; Berendsen, H. J. C. Simulation of Water Transport through a Lipid Membrane. *J. Phys. Chem.* **1994**, *98*, 4155–4168.
- (54) Sugii, T.; Takagi, S.; Matsumoto, Y. A Molecular-Dynamics Study of Lipid Bilayers: Effects of the Hydrocarbon Chain Length on Permeability. *J. Chem. Phys.* **2005**, *123*, 184714.
- (55) Paula, S.; Volkov, A. G.; van Hoek, A. N.; Haines, T. H.; Deamer, D. W. Permeation of Protons, Potassium Ions, and Small Polar Molecules through Phospholipid Bilayers as a Function of Membrane Thickness. *Biophys. J.* **1996**, *70*, 339–348.
- (56) Jansen, M.; Blume, A. A Comparative-Study of Diffusive and Osmotic Water Permeation across Bilayers Composed of Phospholipids with Different Head Groups and Fatty Acyl Chains. *Biophys. J.* **1995**, *68*, 997–1008.
- (57) Evans, E.; Heinrich, V.; Ludwig, F.; Rawicz, W. Dynamic Tension Spectroscopy and Strength of Biomembranes. *Biophys. J.* **2003**, *85*, 2342–2350.